A tomographic method to predict forces in a rolling element bearings

J. J. Kent [1], **M. De C. Loures** [1], **A. L. Gower** [1]
[1] University of Sheffield, Department of Mechanical Engineering,
Sheffield, S10 2TN, United Kingdom

Abstract
Typically methods to detect defects in roller bearings rely on measuring vibrations. There has been a lot of work on signal processing to get the clearest sign of defects appearing on different components. Here we ask how can modelling the elastic waves in the raceway, or other cylindrical components, improve methods that monitor roller bearing vibrations. One clear improvement is that we can predict stress profile on the raceway. By describing and solving for the elastic waves we first deduce a method for elastic tomography in a cylindrical case. Then, to significantly reduce the number of sensors required, we show how to use prior information of the source of vibration, such as the contacts from the rollers. We some examples of recovering the traction profile in the bearing raceway.

1 Introduction

Roller bearings are an integral part of modern industrial machinery, their main purpose is to reduce friction and constrain the motion of rotating components. Roller bearing are everywhere from bicycles to wind turbines to jet engines [1]. Their maintenance remains an important industrial problem and an active field of study [2].

The foremost methods in monitoring the condition of roller bearings are based on vibration analysis, that is: performing a frequency space decomposition of ultrasonic vibration signals measured from the bearing. In particular, the benchmark method in this field is envelope spectrum analysis, where the signal is transformed to frequency and band-pass filtered to show only content in the range of characteristic defect frequencies [3, 4]. On this basis, certain features and diagnoses of bearing defects can be ascertained such as the component that is defective [3].

Current methods for condition monitoring for roller bearings do reduce costs of maintenance and can identify major defects. The field has developed from the simplest possible semi-empirical models, and added complexity as needed. Current methods can diagnoses whether there is defect in the inner or outer race, or on the rollers themselves, and whether the defects are small or extensive in size. However, these methods cannot give detailed information about the stress in the bearing or the precise location of local faults. Further there are many cases for which the vibration response is not well understood, this means that while localised faults might be identified by these methods, the underlying causes of these faults remain unknown [5].

Some work has been done on modelling the vibration response measured from point defects [6, 7]. This work has been shown to be a good model for the vibration response [8]. We expand upon this work by incorporating the physics of elastic wave propagation to provide a more detailed picture of the stress induced by various kinds of defects. In a broad sense, we seek to translate modern methods for inverse problems for elastic waves to the context of monitoring roller bearings, and by doing so develop new methods to predict the stress and detailed description of the faults.

In this paper, we show theoretical and numerical results on how to recover detailed stress information which may improve the early detection and diagnosis of bearing defects. To achieve this, we consider and model elastic waves in a thick cylinder case.

2 Forward Modelling

2.1 General solutions

For a homogeneous and approximately isotropic material, such as many grades of steel are, the elastic waves in the raceway are described by the Navier equation [9][10]

$$\frac{\partial^2 \boldsymbol{u}}{\partial t^2} = c_p^2 \nabla(\nabla \cdot \boldsymbol{u}) - c_s^2 \nabla \times (\nabla \times \boldsymbol{u}), \tag{2.1}$$

where c_p and c_s are the wave speeds for P and S-waves respectively and $\boldsymbol{u}$ is displacement.

To find general solutions to (2.1) we apply a Helmholtz decomposition

$$\boldsymbol{u} = \nabla\phi + \nabla \times (\psi \hat{\boldsymbol{z}}) \quad \text{with} \quad \nabla \cdot (\psi \hat{\boldsymbol{z}}) = 0. \tag{2.2}$$

Applying separation of variables on ϕ and ψ with the Helmholtz decomposition in (2.2) in equation (2.1), leads to the following time-harmonic solutions

$$\phi(r,\theta) = \sum_{n=-\infty}^{\infty} \left(a_n \mathrm{J}_n(k_p r) + b_n \mathrm{H}_n^{(1)}(k_p r) \right) \mathrm{e}^{\mathrm{i}n\theta}, \tag{2.3}$$

$$\psi(r,\theta) = \sum_{n=-\infty}^{\infty} \left(c_n \mathrm{J}_n(k_s r) + d_n \mathrm{H}_n^{(1)}(k_s r) \right) \mathrm{e}^{\mathrm{i}n\theta}. \tag{2.4}$$

Where J_n and $\mathrm{H}_n^{(1)}$ are first kind Bessel and Hankel functions respectively.

2.2 Boundary conditions

The coefficients a_n, b_n, c_n, and d_n in (2.4) can be determined from boundary conditions. We call the *forward problem* the case where the traction on the inside and outside of the raceway are given. We consider this case first before turning to more general boundary conditions.

We begin our considerations by finding an expression for the traction at a boundary. Since we model the bearing raceway as being made from a homogeneous, isotropic material the Cauchy stress tensor is given by

$$\boldsymbol{\sigma} = \lambda \mathrm{tr}(\boldsymbol{\varepsilon})\mathbf{I} + 2\mu\boldsymbol{\varepsilon}$$

where λ and μ are the Lame parameter and shear modulus of the material respectively, these are related to the wave speeds c_p and c_s via $c_p^2 = \frac{\lambda+2\mu}{\rho}$ and $c_s^2 = \frac{\mu}{\rho}$, and $\boldsymbol{\varepsilon}$ is the strain tensor.

Further, the unit normal out of the material will be $-\hat{\boldsymbol{r}}$ for $r = r_1$ and $\hat{\boldsymbol{r}}$ for $r = r_2$, where $\hat{\boldsymbol{r}}$ is the unit vector in the radial direction. Hence, we find that the traction, $\boldsymbol{\tau}$, on a boundary is given by

$$\boldsymbol{\tau} = \boldsymbol{\sigma} \cdot \hat{\boldsymbol{r}} = \sigma_{rr}\hat{\boldsymbol{r}} + \sigma_{r\theta}\hat{\boldsymbol{\theta}} \tag{2.5}$$

where σ_{rr} and $\sigma_{r\theta}$ the normal and shear stresses acting along the radial direction. These components are calculated from the Cauchy strain tensor given above.

In our problem, we have two boundaries; one that is in contact with the rolling elements at $r = r_1$ and another that forms the outer boundary of the bearing at $r = r_2$, this can be seen in figure 1.

Let the traction on the boundary $r = r_1$, $\boldsymbol{\tau}^1(\theta)$, and the traction on the boundary $r = r_2$, $\boldsymbol{\tau}^2(\theta)$, be given by:

$$\boldsymbol{\tau}^1(\theta) = -p^1(\theta)\hat{\boldsymbol{r}} - s^1(\theta)\hat{\boldsymbol{\theta}}, \tag{2.6}$$

$$\boldsymbol{\tau}^2(\theta) = p^2(\theta)\hat{\boldsymbol{r}} + s^2(\theta)\hat{\boldsymbol{\theta}}, \tag{2.7}$$

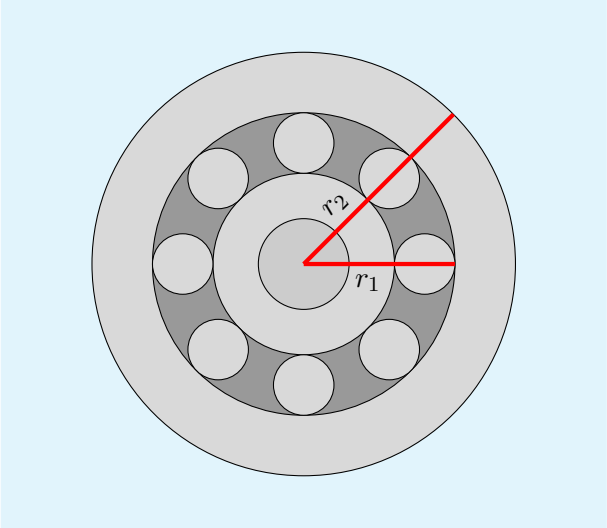

Figure 1: Figure illustrates bearing geometry

where $p^1(\theta)$, $s^1(\theta)$, $p^2(\theta)$ and $s^2(\theta)$ are given by the following Fourier series

$$p^1(\theta) = \sum_{n=-\infty}^{\infty} p_n^1 \mathrm{e}^{\mathrm{i}n\theta}, \quad s^1(\theta) = \sum_{n=-\infty}^{\infty} s_n^1 \mathrm{e}^{\mathrm{i}n\theta}, \tag{2.8}$$

$$p^2(\theta) = \sum_{n=-\infty}^{\infty} p_n^2 \mathrm{e}^{\mathrm{i}n\theta}, \quad s^2(\theta) = \sum_{n=-\infty}^{\infty} s_n^2 \mathrm{e}^{\mathrm{i}n\theta}. \tag{2.9}$$

Hence, substituting the potentials (2.3) and (2.4) into the equations for σ_{rr} and $\sigma_{r\theta}$, we arrive at a matrix equation for the coefficients $\boldsymbol{a}_n = (a_n, b_n, c_n, d_n)^{\mathrm{T}}$ of the potentials ϕ and ψ,

$$\mathbf{M}_n^{\text{for}} \boldsymbol{a}_n = \boldsymbol{f}_n \tag{2.10}$$

where $\boldsymbol{f}_n = (p_n^1, s_n^1, p_n^2, s_n^2)^{\mathrm{T}}$. From this, we can infer that, given the matrix $\mathbf{M}_n^{\text{for}}$ is non-singular, $\boldsymbol{a}_n$ is given by

$$\boldsymbol{a}_n = \left(\mathbf{M}_n^{\text{for}}\right)^{-1} \boldsymbol{f}_n.$$

In the next section, we show how we may use the above to model loading and defects in roller bearings.

2.3 Modelling loading and defects

We now come to modelling loading and defects. In a roller bearing under any loading, we find that the load on the bearings can be described as follows

$$y(\theta, t) = L(\theta) d(\theta, t), \quad \text{where} \quad d(\theta, t) = \sum_{s=-\infty}^{\infty} \delta\left(\theta + \frac{2\pi s}{Z} - \Omega t\right), \tag{2.11}$$

the function $L(\theta)$ is called the loading-distribution or loading profile, it describes how the load supported by the bearing is distributed among the rollers; in the case of radial loading the loading profile is given by the Stribeck equation, details can be found in [6, 7, 1]. The term $d(\theta, t)$ represents the point contacts between the rollers and the bearing raceway, where we assumed the area of the contact between the rollers and the bearing raceway is small compared to the radii of the rollers and the bearing raceway. This allows us to approximately modelled the contact force as a Dirac delta [1, 11]. The meaning of (2.11) is illustrated in

figures 2a and 2b.

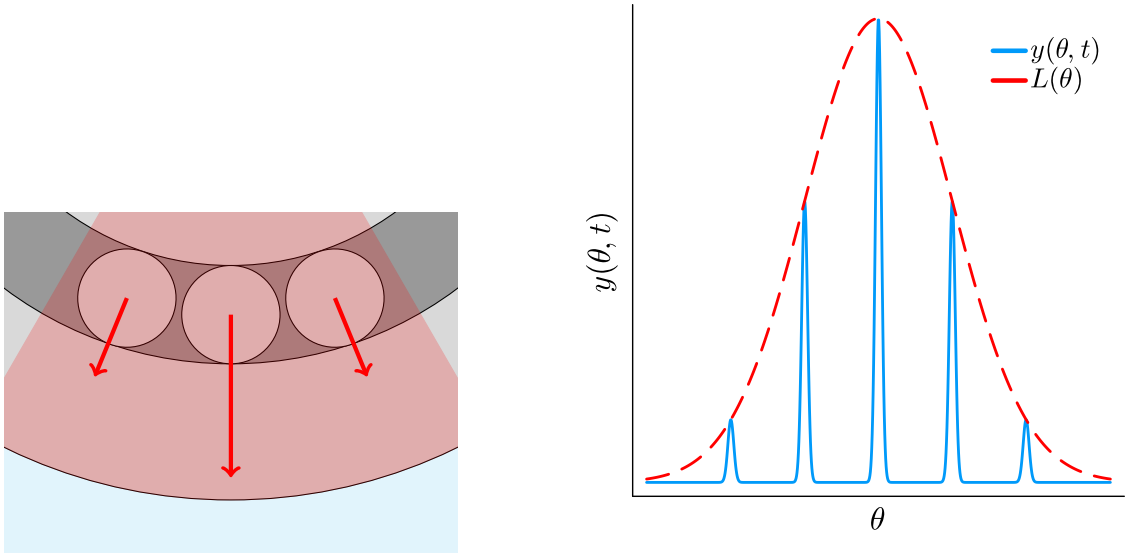

(a) The function $L(\theta)$ determines how much load rollers in the loading zone, the red area in the figure, experience.

(b) Visualisation of equation (2.11). Note that Dirac deltas are shown using sharp Gaussians for illustrative purposes.

Figure 2: Figure 2a shows the meaning of (2.11) in relation the bearing system. Figure 2b shows the relation between the loading profile L and the forcing y.

In the example presented, we take

$$L(\theta) = 10\exp\left(-\frac{\left(\theta - \frac{3\pi}{2}\right)^2}{0.18}\right)$$

we note here that this L is taken for illustrative purposes, as its a smooth function that allows us to mark out a distinct loading zone with ease, as illustrated in figure 3:

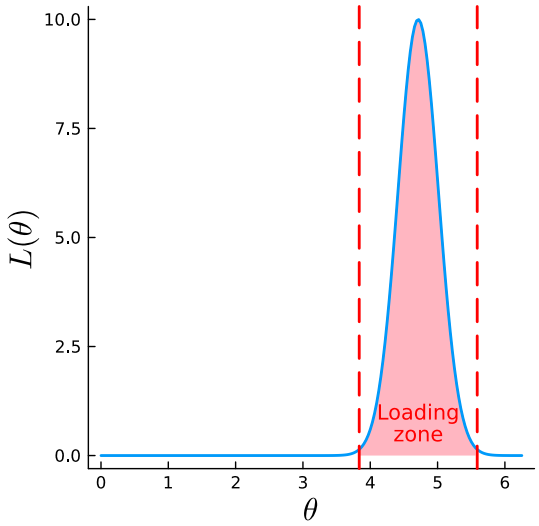

Figure 3: Loading profile with location of loading zone marked.

The parameter values taken for the simulations performed in this work can be found in table 1. With these parameters, and the forcing illustrated in figure 3, we can create a time simulation of the stress due to the

bearings rolling around.

Table 1: Parameter values used in simulations

Parameter	value	units
r_1	1.0	m
r_2	2.0	m
c_p	5.0	m/s
c_s	3.5	m/s
ρ	7.8	kg/m^3
Ω	3.5	rads/s
Z	8	N/A

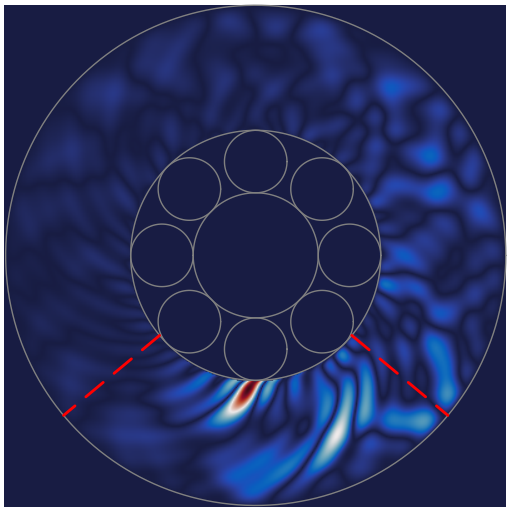

Figure 4: $|\mathcal{F}^{-1}\{\phi\}|$ for $t = 0$. Shows a roller entering the load zone marked out by the red dashed lines; releasing stress waves.

The formalism introduced also allows us to add defects which are periodically struck by the rollers. To do this, we modify equation (2.11) to be

$$y(\theta, t) = f(\theta)d(\theta, t), \quad \text{where} \quad f(\theta) = L(\theta)(1 + A\delta(\theta - \theta_0)), \tag{2.12}$$

this mirrors the case of a modulated point defect in [6]. Figure 5 shows the $f(\theta)$ used in our simulations;

as before we can perform a time simulation to model the field in the bearing due to the point defect, this is shown in figure 6

thus far we have undertaken forward modelling and illustrated how we might model loading and defects in roller bearings. In the coming sections we turn our attention to the inverse problem; namely, detecting and diagnosing defects based on passive ultrasound measurements.

3 Inverse problem

3.1 Naive inversion

In the previous section, we constructed particular solutions for the vibrations of the outer-raceway knowing the traction on both boundaries. In practice, we will not have access to the traction on the inner-boundary,

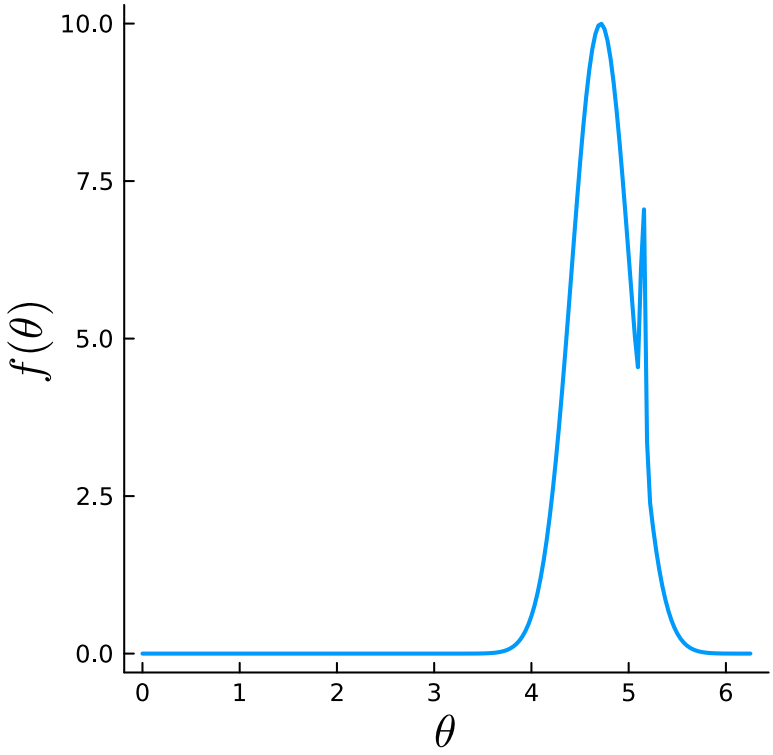

Figure 5: Loading profile with a periodic point defect. Note that we have opted to model the Dirac delta as a sharp Gaussian.

we will only have access to measured vibrations, i.e., displacement and traction on the outer-boundary. As such, it is worth investigating what we can recover knowing these quantities.

We will assume, for the time being, that we have access to the vibrations and traction on the whole outer-boundary.

We can describe the displacement on the outer-boundary using a Fourier series

$$\boldsymbol{u}(r_2, \theta) = \boldsymbol{u}^2(\theta) = \sum_n \left(u_n^{(r)} \hat{\boldsymbol{r}} + u_n^{(\theta)} \hat{\boldsymbol{\theta}} \right) \mathrm{e}^{\mathrm{i}n\theta}$$

using this boundary data and the expression for $\boldsymbol{u}$ found in equation (2.2), we may alter the matrix found in equation (2.10) to

$$\mathbf{M}_n^{\mathrm{inv}} \boldsymbol{a}_n = \boldsymbol{u}_n \tag{3.1}$$

where $\boldsymbol{u}_n = (u_n^{(r)}, u_n^{(\theta)}, p_n^2, s_n^2)^{\mathrm{T}}$. Hence, we find that

$$\boldsymbol{a}_n = \left(\mathbf{M}_n^{\mathrm{inv}} \right)^{-1} \boldsymbol{u}_n.$$

With this in place, one might expect that this is the last word on the problem of recovering stress. It seems, with some simple mathematical modelling we can recover everything. However, let us turn back to our examples. Recall that in section 2.3, we modelled the vibrations for a healthy bearing and for a bearing with a point defect. Let us see how well naive inversion recovers the stress for these cases.

As can be seen in figure 8, the recovery of the loading profile with naive inversion is quite poor. This is because we need to access a larger number of modes in order to recover the loading profile properly as the information pertaining to it is shifted to higher order modes.

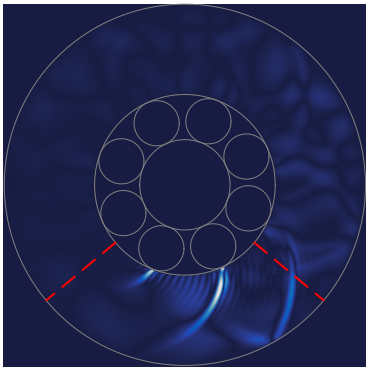

(a) Time simulation for periodic point defect, $t = 0$

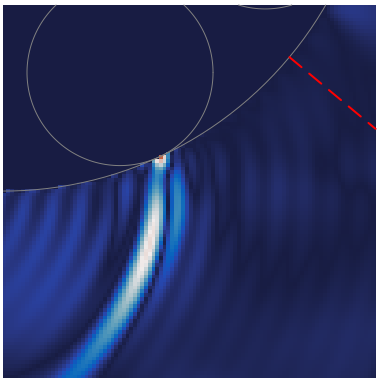

(b) Zoomed in view on defect location.

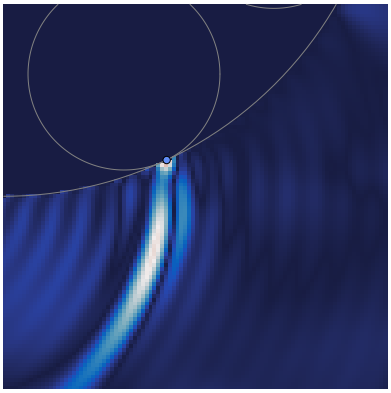

(c) Zoomed in view on defect location with defect location marked.

Figure 6: $|\mathcal{F}^{-1}\{\phi\}|$ at $t = 0$ for a point defect

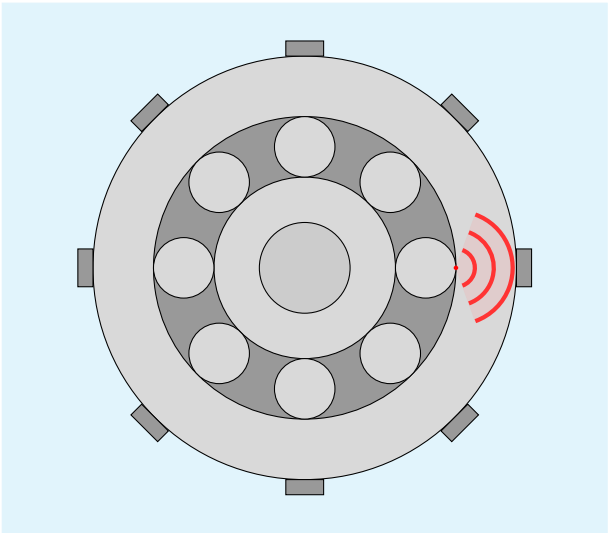

Figure 7: Vibrations from a bearing striking a defect on the boundary at $r = r_1$ measured by an array of sensors on the boundary at $r = r_2$

However, when one looks at the case of the point defect, we find that Naive inversion is able to recover some features quite well as shown in figure 9.

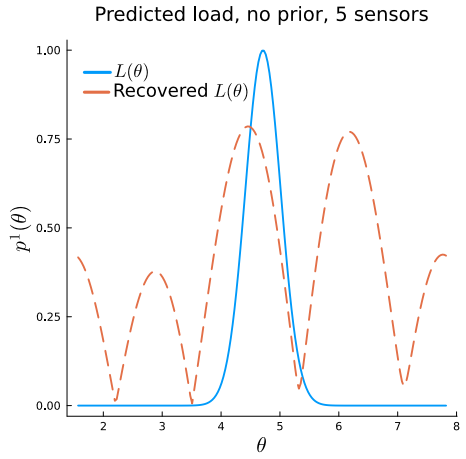

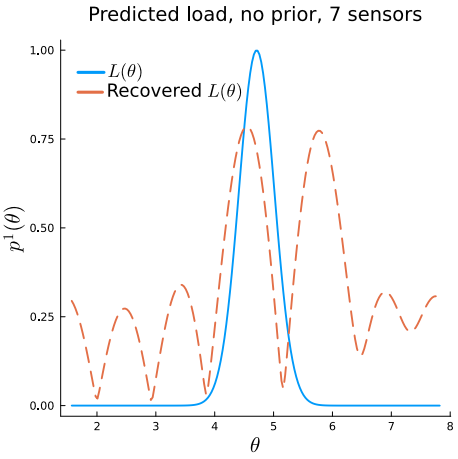

(a) Naive inversion of loading profile with 5 measurements.(b) Naive inversion of loading profile with 7 measurements.

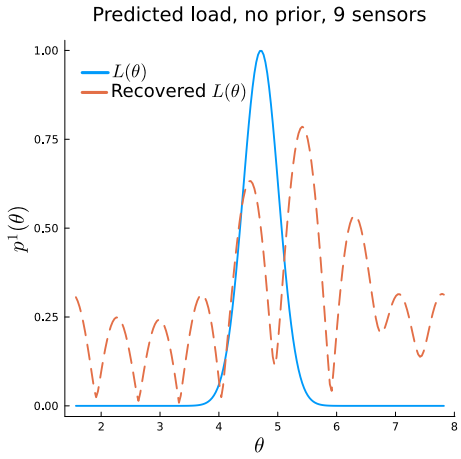

(c) Naive inversion of loading profile with 9 measurements.

Figure 8: Naive inversion to recover the loading profile. Note that amplitudes have been normalised.

this is because the point defect remains in a fixed location and therefore does not introduce a mode shift, this means that naive inversion can recover this reasonably well, in particular at high frequencies.

This section has demonstrated that naive inversion is well suited to locating point defects, however, it is not capable of reliably recovering the loading profile. In the next section, we show how incorporating basic prior information can improve the inversion.

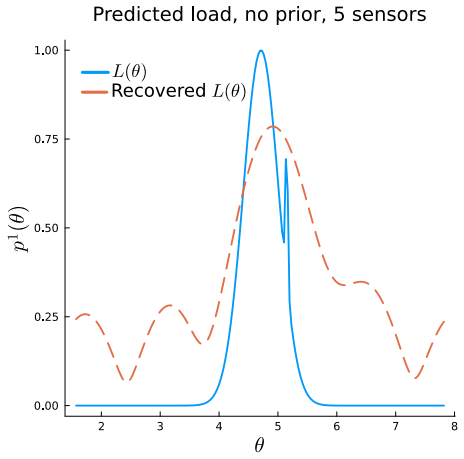

(a) Naive inversion of point defect with 5 measurements.

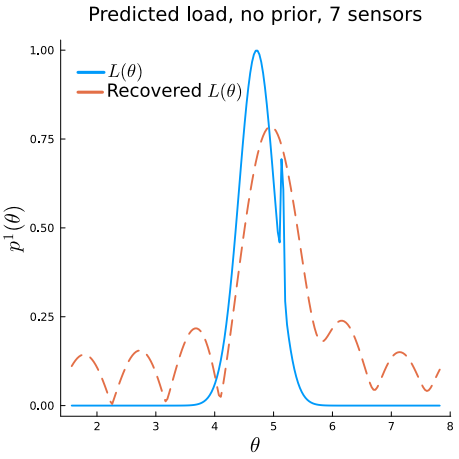

(b) Naive inversion of point defect with 7 measurements.

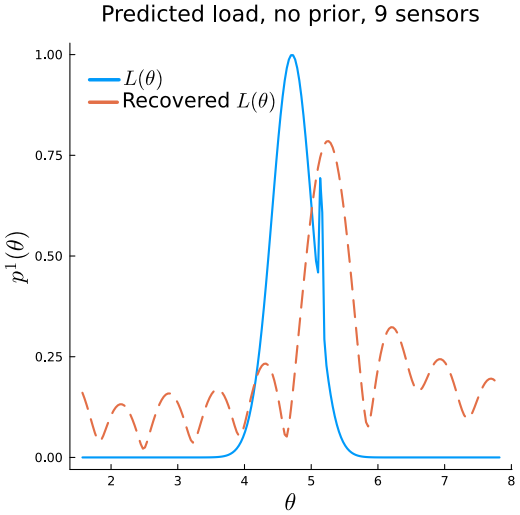

(c) Naive inversion of point defect with 9 measurements.

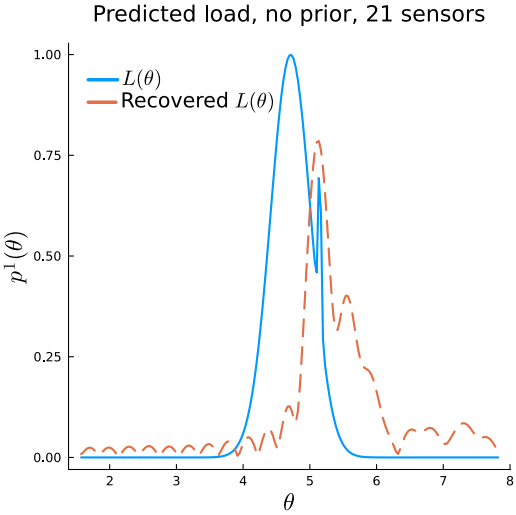

(d) Naive inversion of point defect with 21 measurements.

Figure 9: Naive inversion to recover the point defect. Note that amplitudes have been normalised

3.2 Prior method

The system described by 3.1 works for any traction and displacement boundary conditions. If we knew that solution, for example, was due to rollers in contact with the raceway, we could use this prior knowledge to either improve the accuracy of the solution, or reduce the number of sensors.

Let us describe this idea mathematically. However, before proceeding, we need to introduce some notation. notice that we can write the whole modal system at once for the inverse problem as

$$\mathbf{M}^{\text{inv}} = \text{diag}(\dots, \mathbf{M}^{\text{inv}}_{-1}, \mathbf{M}^{\text{inv}}_{0}, \mathbf{M}^{\text{inv}}_{1}, \dots), \tag{3.2}$$

$$\boldsymbol{a} = \begin{bmatrix} \vdots \\ \boldsymbol{a}_{-1} \\ \boldsymbol{a}_0 \\ \boldsymbol{a}_1 \\ \vdots \end{bmatrix}, \quad \boldsymbol{u} = \begin{bmatrix} \vdots \\ \boldsymbol{u}_{-1} \\ \boldsymbol{u}_0 \\ \boldsymbol{u}_1 \\ \vdots \end{bmatrix}, \tag{3.3}$$

which results in the block system

$$\mathbf{M}^{\text{inv}}\boldsymbol{a} = \boldsymbol{u}, \tag{3.4}$$

and analogously for the forward problem as

$$\mathbf{M}^{\text{for}}\boldsymbol{a} = \boldsymbol{f}. \tag{3.5}$$

We can now describe the prior method. In general, we consider that the field coefficients $\boldsymbol{a}$ can be parameterised as

$$\boldsymbol{a} = \mathbf{B}\boldsymbol{x} + \boldsymbol{c}, \tag{3.6}$$

where $\mathbf{B}$ and $\boldsymbol{c}$ contain the prior information about the system and $\boldsymbol{x}$ is the unknowns of the system.

For example, in the simplest case, our prior information might be the number of bearings Z and the angular speed, Ω at which they rotate. Thus, using equation (2.11) we can form a simple prior.

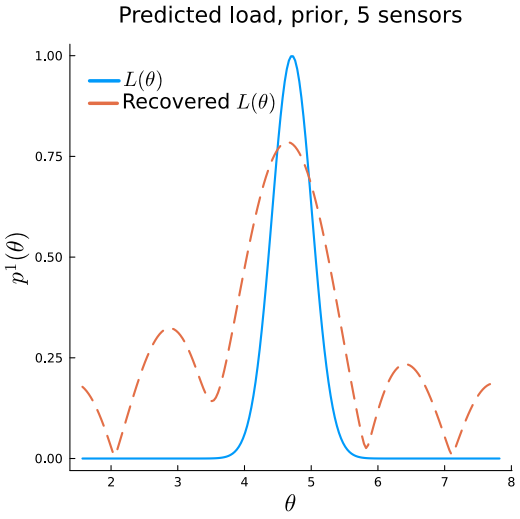

(a) Inversion of loading profile with 5 measurements.

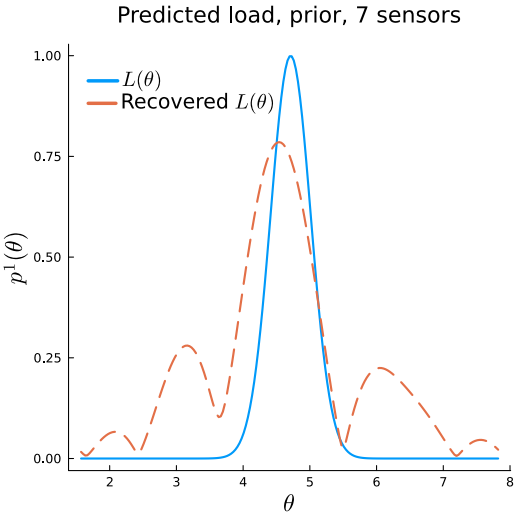

(b) Inversion of loading profile with 7 measurements.

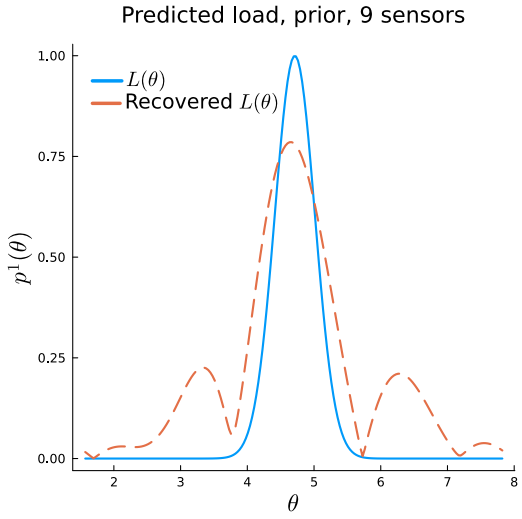

(c) Inversion of loading profile with 9 measurements.

Figure 10: Inversion to recover the loading profile using the prior method. Note that amplitudes have been normalised.

The figure 10 demonstrates the power of using even the simplest available prior information. We find that for relatively low numbers of sensors we are able to recover information about the loading profile, simply from measurements of vibrations.

4 Conclusions

Here we show the first steps in developing a method to predict the stress, or traction, on rollers in a bearing by measuring elastic waves. To develop this method, we develop a mathematical method to describe how waves propagate in a thick walled cylindrical tube, which is a good approximation to the raceway in most roller bearings.

By explicitly modelling the elastic waves we can make better use of all the information available. For example, we show how to include prior knowledge on the origin of the stress, and elastic waves. In this case, the point contacts between the rollers and raceway. By using this prior knowledge, we are able to greatly improve the recovery of the loading on the bearings with fewer sensors, as shown in Figure 10 which can be compared with Figure 8 which does not use any prior knowledge.

The next steps will be to adjust the method for most realistic forcing on the bearings, and study how robust this methods are when given noisy measurements.

Acknowledgements

This work has been supported by EPSRC, Engineering and Physical Sciences Research Council.

References

[1] T. Harris, *Rolling Bearing Analysis*, ser. A Wiley-interscience publication. Wiley, 2001. [Online]. Available: https://books.google.co.uk/books?id=Pt9SAAAAMAAJ

[2] E. Hart, A. Turnbull, J. Feuchtwang, D. McMillan, E. Golysheva, and R. Elliott, "Wind turbine main-bearing loading and wind field characteristics," *Wind Energy*, vol. 22, no. 11, pp. 1534–1547, 2019.

[3] R. Randall, *Vibration-based Condition Monitoring: Industrial, Automotive and Aerospace Applications*. Wiley, 2021. [Online]. Available: https://books.google.co.uk/books?id=InoqEAAAQBAJ

[4] A. Rezaei, "Fault detection and diagnosis on the rolling element bearing," Thesis, Carleton University, 2007.

[5] I. Howard, "A review of rolling element bearing vibration "detection, diagnosis and prognosis"," 10 1994.

[6] P. McFadden and J. Smith, "Model for the vibration produced by a single point defect in a rolling element bearing," *Journal of Sound and Vibration*, vol. 96, no. 1, pp. 69–82, 1984.

[7] P. McFadden and J. Smith, "The vibration produced by multiple point defects in a rolling element bearing," *Journal of Sound and Vibration*, vol. 98, no. 2, pp. 263–273, 1985.

[8] T. Zoladz, E. Earhart, and T. Fiorucci, "Bearing defect signature analysis using advanced non-linear signal analysis in a controlled environment," NASA Technical Memorandum, Tech. Rep. 108491, 1995.

[9] P. M. Shearer, *Introduction to Seismology*. Cambridge; New York: Cambridge University Press, 2009.

[10] P. Howell, G. Kozyreff, and J. R. Ockendon, *Applied Solid Mechanics*. Cambridge, UK; New York: Cambridge University Press, 2009.

[11] P. Mora, F. Treyssède, and L. Laguerre, "Elastic response of a cylinder loaded by a hertzian contact pressure and maintained in equilibrium by its inertia," *Proceedings of the Royal Society A: Mathematical, Physical and Engineering Sciences*, vol. 480, no. 2287, p. 20230891, 2024. [Online]. Available: https://royalsocietypublishing.org/doi/abs/10.1098/rspa.2023.0891

Appendix

A Nomenclature

$\boldsymbol{u}$	displacement vector
ϕ	pressure potential
ψ	shear potential
c_p	pressure speed
c_s	shear speed
J_n	Bessel function of order n
$\mathrm{H}_n^{(1)}$	Hankel function of order n of the first kind
λ	lame parameter
$\boldsymbol{\tau}$	traction
μ	shear modulus
$\boldsymbol{\sigma}$	Stress tensor
$\boldsymbol{\varepsilon}$	Strain tensor
$\mathbf{M}^{\mathrm{for}}$	forward governing matrix
$\mathbf{M}^{\mathrm{inv}}$	inverse governing matrix
$\boldsymbol{a}_n$	field coefficients for each mode
$\boldsymbol{f}_n$	boundary data vector for forward problem
$\boldsymbol{u}_n$	boundary data vector for inverse problem
$y(\theta, t)$	pressure traction on boundary
$d(\theta, t)$	Dirac comb of the moving rollers
δ	Dirac delta
$L(\theta)$	Loading profile without crack
$f(\theta)$	Loading profile with crack
Z	Number of rollers
r_1	Inner radius
r_2	Outer radius